Application of a simple algorithm to estimate daily evapotranspiration from NOAA–AVHRR images for the Iberian Peninsula

J.A. Sobrino [a],[*], M. Gómez [a],[1], J.C. Jiménez-Muñoz [a],[1], A. Olioso [b]

[a] *Department of Thermodynamics, Faculty of Physics, University of Valencia, 50 Dr. Moliner, 46100 Burjassot, Spain*
[b] *INRA Bioclimatologie, Domaine Saint-Paul, Avignon, France*

Abstract

Evapotranspiration (ET) is a key process in land surface–atmosphere studies. It mainly depends on water availability and incoming solar radiation and then reflects the interactions between surface water processes and climate. In this paper, a methodology for retrieving ET from low spatial resolution remote sensing data is presented. It is based on the evaporative fraction concept, and it has been applied to Advanced Very High Resolution Radiometer (AHVRR) data acquired over the Iberian Peninsula. The methodology does not require other data than the data provided by the satellite and may be applied to areas with almost spatially constant atmospheric conditions and which include wet and dry sub-areas. The comparison with high resolution ET estimation shows a root mean square error (RMSE) of 1.4 mm d^{-1} which is in agreement with the sensitivity analysis of the method. Finally, the methodology has been applied to temporal NOAA–AVHRR images acquired from 1997 to 2002 in order to analyze the seasonal evolution of the daily ET. The temporal study of the ET values realized in this paper shows that the highest ET values are associated with the higher development crops, while the lowest values are related with lower development or null crop. As a conclusion, it is shown that the ET values obtained with the proposed model evolve according to the variations presented in parameters such as surface temperature or vegetation index.

1. Introduction

Continuous evapotranspiration (ET) measurements at different scales are important in hydrology and agriculture, and also in other environmental studies. ET is a key process in land surface–atmosphere studies. It mainly depends on water availability and incoming solar radiation and then reflects the interactions between surface water processes and climate. Over the last years, the scientific community has been interested in estimating evapotranspiration by remote sensing, since it is the unique way to retrieve ET at several temporal and spatial scales. For this reason, different methods have been developed to derive surface fluxes from remote sensing observations, such as:

SEBAL (Surface Energy Balance Algorithm for Land, Bastiaanssen, 2000; Bastiaanssen et al., 1998a,b; Jacob et al., 2002), S-SEBI (Simplified Surface Energy Balance Index, Roerink et al., 2000), SEBS (Surface Energy Balance System, Jia et al., 2003; Su, 2002) and TSEB (Two-Source Energy Balance, French et al., 2003; Kustas & Norman, 1999; Norman et al., 1995).

In Sobrino et al. (2005) and Gómez et al. (2005) a simple method for retrieving daily ET from high resolution data based on the S-SEBI model was proposed, which is a simple way to derive evapotranspiration from evaporative fraction concept. It is based on the estimation of the evaporative fraction from the contrast between dry and wet areas according to Roerink et al. (2000). The purpose of this paper is to adapt this methodology to the low spatial resolution data provided by the Advanced Very High Resolution Radiometer (AVHRR) on board of the National Oceanic and Atmospheric Administration (NOAA) platform. The paper is organized as follows: Section 2 describes how instantaneous and daily ET are retrieved from NOAA–

* Corresponding author. Tel.: +34 963543115; fax: +34 96 354 3099.
E-mail addresses: sobrino@uv.es (J.A. Sobrino), monica.gomez@uv.es (M. Gómez), juancar.jimenez@uv.es (J.C. Jiménez-Muñoz), olioso@avignon.inra.fr (A. Olioso).
[1] Fax: +34 96 354 3099.

Table 1
Equations used to estimate the daily ET from high and low resolution images

Albedo	$\alpha = 0.5\,\rho_{NIR} + 0.5\,\rho_{RED}$ AVHRR: ρ_{RED} and ρ_{NIR} are calculated using channel 1 (0.63 μm) and channel 2 (0.91 μm). DAIS: ρ_{RED} and ρ_{NIR} are calculated using channel 10 (0.66 μm) and channel 22 (0.87 μm).
Emissivity	AVHRR: Land surface emissivity estimated from NOAA–AVHRR data using the NDVI Thresholds method (Sobrino & Raissouni, 2000). DAIS: Land surface emissivity estimated from DAIS data using the NEM (Normalized Emissivity Method) developed by Gillespie (1985) (Sobrino et al., 2002).
Surface temperature	AVHRR: $T_S = T_4 + 1.40(T_4 - T_5) + 0.32(T_4 - T_5)^2 + 0.83 + (57 - 5W)(1 - \varepsilon) - (161 - 30W)\Delta\varepsilon$ T_4 and T_5 are the at-sensor or brightness temperature (In K) for NOAA–AVHRR thermal channels 4 (10.3–11.3 μm) and 5 (11.5–12.5 μm). DAIS: $T_S = T_{77} + 2.082(T_{77} - T_{78}) + 0.033(T_{77} - T_{78})^2 + 56.672(1 - \varepsilon) - 109.429\Delta\varepsilon - 0.06$ T_{77} and T_{78} are the at-sensor or brightness temperature (in K) for DAIS thermal channels 77 (11.266 μm) and 78 (11.997 μm).

Net radiation flux	$R_n = (1 - \alpha)R_{c\lambda\downarrow} + \varepsilon R_{g\lambda\downarrow} - \varepsilon\sigma T_S^4$
	 AVHRR:
	   $R_{c\lambda\downarrow} = \tau_T S$, τ_T is the total transmissivity,
	 S is the solar constant.
	   $\varepsilon R_{g\lambda\downarrow} \approx C\varepsilon\sigma T_S^4$ (Hurtado & Sobrino, 2001)
	 DAIS: $R_{c\lambda\downarrow}$ and $R_{g\lambda\downarrow}$, are the incoming shortwave and longwave radiation, respectively; obtained from meteorological data.

Soil heat flux	$G = R_n 0.5 \exp(-2.13\,\mathrm{MSAVI})$
Evaporative fraction	$\Lambda = \dfrac{T_H - T_S}{T_H - T_{LE}}$
Heat latent flux	$\mathrm{LET} = \Lambda(R_n - G)$
Daily ET	$\mathrm{ET}_d = \dfrac{\Lambda C_{di}}{L} R_n$

AVHRR data, Section 3 shows the available imagery and Section 4 presents the results obtained, including a sensitivity analysis of the method, the test of the method by comparing low resolution estimations of ET to high resolution ones, and also monthly and seasonal analysis of ET over the Iberian peninsula for several years. The main conclusions drawn from this study are presented in Section 5.

2. Methods

2.1. Instantaneous evapotranspiration

The method proposed in this paper for instantaneous ET estimation from NOAA–AVHRR data is based on the Simplified Surface Energy Balance Index (S-SEBI) model and the evaporative fraction (Λ) concept proposed by Roerink et al. (2000), in which the latent heat flux (LET) is given by:

$$\mathrm{LET}_i = \Lambda_i(R_{ni} - G_i) \tag{1}$$

where R_n is the net radiation flux and G is the soil heat flux. The subscript 'i' refers to instantaneous values, and units for heat
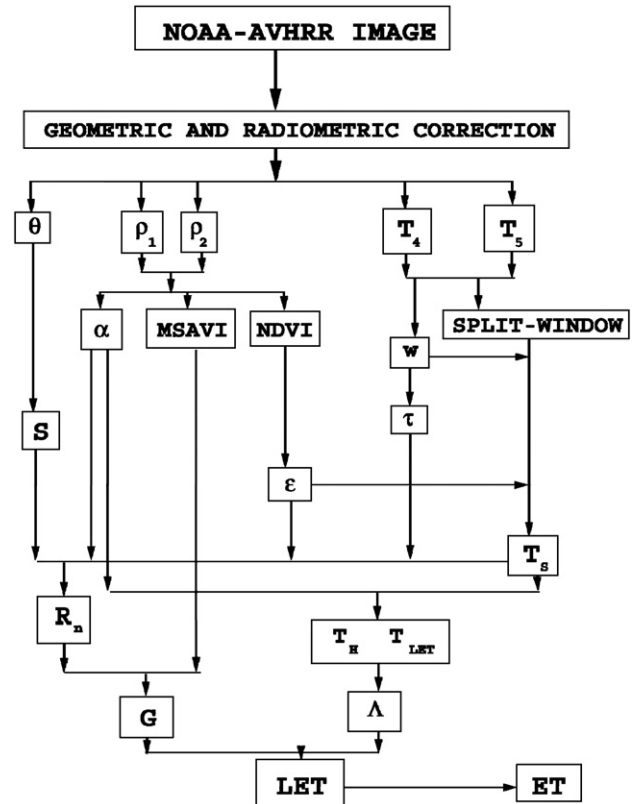
Fig. 1. Flowchart of the proposed methodology to obtain evapotranspiration from NOAA–AVHRR data.

and net radiation fluxes are given in W m^{-2}. The soil heat flux (G) can be obtained from the Modified Soil Adjusted Vegetation Index (MSAVI) (Sobrino et al., 2005), whereas the evaporative fraction (Λ) is obtained from the scatterplot between surface temperature and albedo (Roerink et al., 2000). The net radiation flux (R_n) is estimated from the radiation balance for all incoming and outgoing radiation (see Table 1 and Fig. 1). Table 1 shows that the net radiation flux
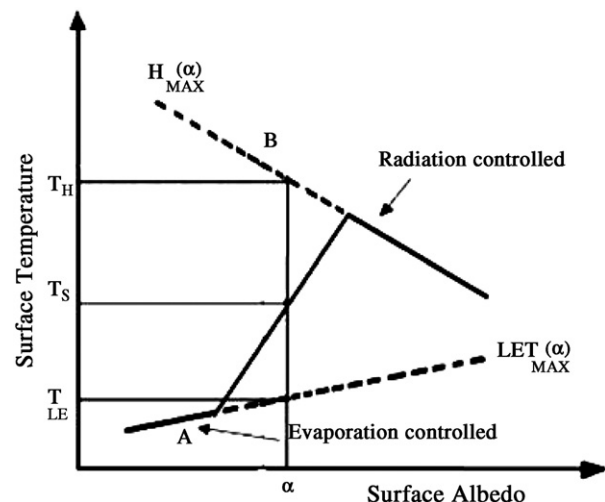
Fig. 2. Surface temperature versus surface albedo. H is the sensible heat flux, LET is the latent heat flux and α is the albedo (adapted from Roerink et al., 2000).
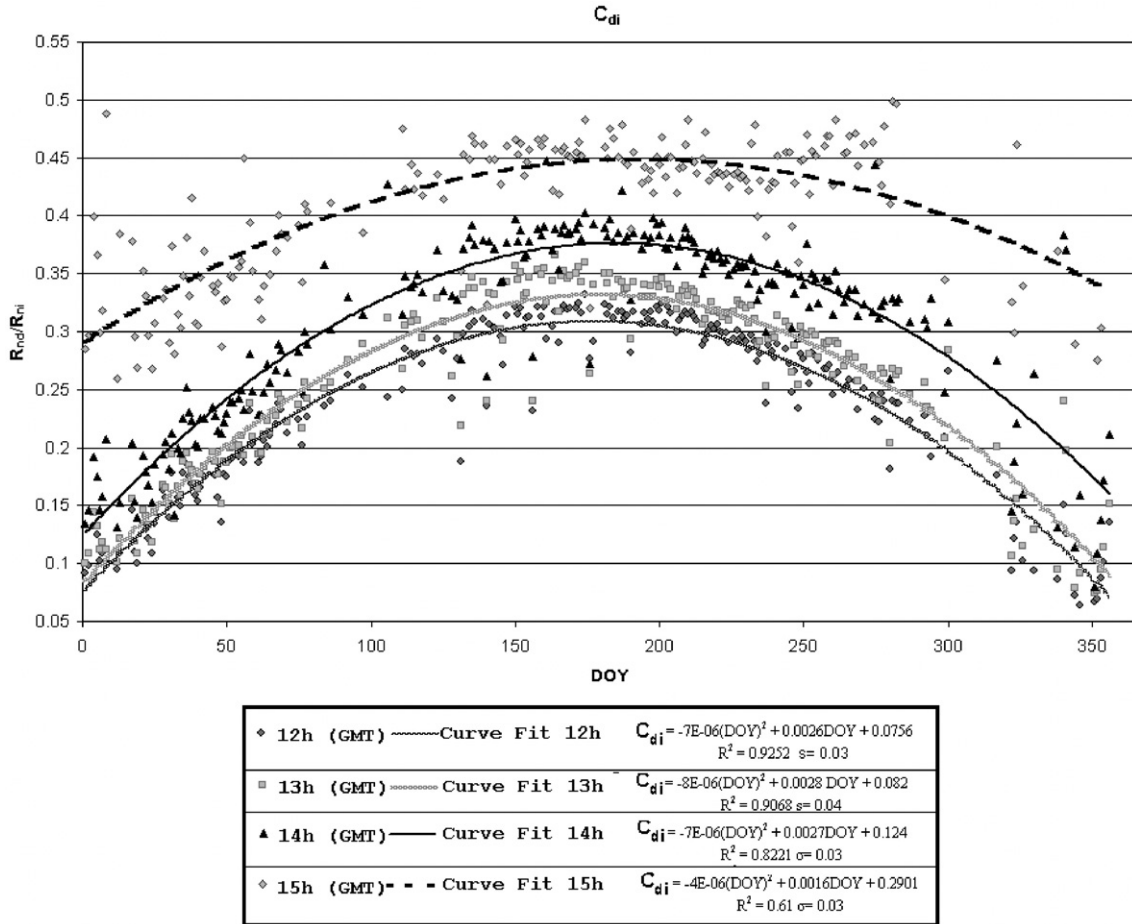
Fig. 3. Ratio (C_{di}) between daily net radiation (R_{nd}) and instantaneous (R_{ni}) net radiation ($C_{di} = R_{nd}/R_{ni}$) versus the day of the year (DOY) and different times. The expressions were obtained from net radiation fluxes measured in 2000 at the meteorological station of the "El Saler" area, located in the East coast of the Iberian Peninsula (Valencia, 39° 20′ 41.165″ N, 0° 19′ 12.031″ W, at sea level). The correlation coefficient (R^2) and the standard error of estimation (σ) are also given.

can be obtained from albedo (α), total transmissivity (τ_T), the Solar Constant (S), surface broadband emissivity (ε), the incoming longwave radiation ($R_{g\lambda\downarrow}$) and surface temperature (T_S). In order to estimate the net radiation flux according to the equation shown in Table 1, an empirical relationship

Table 2
Ratio between daily and instantaneous net radiation (C_{di}) for AVHRR images acquired in 1999

Date and time (aa/mm/dd_hh)	C_{di}	Date and time (aa/mm/dd_hh)	C_{di}
990105_13	0.096	990626_15	0.448
990130_14	0.200	990707_14	0.384
990201_14	0.203	990716_14	0.384
990217_14	0.237	990723_15	0.450
990302_15	0.373	990801_15	0.450
990318_15	0.390	990814_14	0.377
990330_15	0.401	990823_14	0.372
990409_14	0.323	990915_15	0.437
990418_14	0.334	991009_15	0.423
990424_15	0.421	991103_15	0.404
990508_14	0.355	991124_15	0.385
990521_15	0.436	991202_15	0.376
990604_14	0.374		

C_{di} values have been obtained using the relationships presented in Fig. 3.

between atmospheric transmissivity (τ) and atmospheric water vapour content (W) was found using the MODTRAN radiative transfer code (Abreu & Anderson, 1996) and a set of 60 atmospheric soundings described in Sobrino et al. (1993). Low aerosol optical thickness values were assumed. In this way, total shortwave transmittance (0.3–3 μm) could be obtained from water vapour contents (W, in g cm^{-2}) according to:

$$\tau = -0.0268W^2 + 0.0029W + 0.7212 \tag{2}$$

with a standard error of estimation $\sigma = 0.003$ and a correlation coefficient $R^2 = 0.98$. The atmospheric water vapour content had been obtained from AVHRR data, using the Split-Window Covariance Variance Ratio (SWCVR) method (Li et al., 2003; Sobrino et al., 1994, 1999). Fig. 1 shows the flowchart of the proposed method for retrieving ET from NOAA–AVHRR images. Due to the images sizes used in this paper, it is not possible to have constant atmospheric conditions, for this reason, it is necessary use the water vapor values distribution image.

The final step to solve the Eq. (1) is to estimate the evaporative fraction Λ_i. Previous works in the literature focused on the retrieval of evaporative fraction from remote sensing

Table 3
Equations considered in the sensitivity analysis of the daily evapotranspiration estimation

Parameter	Equation
Daily evapotranspiration	$\sigma(\mathrm{ET}_d) = \sqrt{\left\lvert\dfrac{\partial \mathrm{ET}_d}{\partial \Lambda}\sigma(\Lambda)\right\rvert^2 + \left\lvert\dfrac{\partial \mathrm{ET}_d}{\partial C_{di}}\sigma(C_{di})\right\rvert^2 + \left\lvert\dfrac{\partial \mathrm{ET}_d}{\partial R_n}\sigma(R_n)\right\rvert^2} = \sqrt{\left\lvert\dfrac{C_{di}R_n}{L}\sigma(\Lambda)\right\rvert^2 + \left\lvert\dfrac{\Lambda R_n}{L}\sigma(C_{di})\right\rvert^2 + \left\lvert\dfrac{C_{di}\Lambda}{L}\sigma(R_n)\right\rvert^2}$
Net radiation flux	$\sigma(R_n) = \sqrt{\left\lvert\dfrac{\partial R_n}{\partial \alpha}\sigma(\alpha)\right\rvert^2 + \left\lvert\dfrac{\partial R_n}{\partial R_{c\lambda\downarrow}}\sigma(R_{c\lambda\downarrow})\right\rvert^2 + \left\lvert\dfrac{\partial R_n}{\partial R_{g\lambda\downarrow}}\sigma(R_{g\lambda\downarrow})\right\rvert^2 + \left\lvert\dfrac{\partial R_n}{\partial \varepsilon}\sigma(\varepsilon)\right\rvert^2 + \left\lvert\dfrac{\partial R_n}{\partial T_S}\sigma(T_S)\right\rvert^2}$ $= \sqrt{\left\lvert R_{c\lambda\downarrow}\sigma(\alpha)\right\rvert^2 + \left\lvert(1-\alpha)\sigma(R_{c\lambda\downarrow})\right\rvert^2 + \left\lvert(R_{g\lambda\downarrow}-\sigma T_S^4)\sigma(\varepsilon)\right\rvert^2 + \left\lvert\varepsilon\sigma(R_{g\lambda\downarrow})\right\rvert^2 + \left\lvert-4\varepsilon\sigma T_S^3\sigma(T_S)\right\rvert^2}$
Incoming shortwave radiation	$\sigma(R_{c\lambda\downarrow}) = \lvert S\sigma(\tau_T)\rvert$
Incoming longwave radiation	$\sigma(R_{g\lambda\downarrow}) = \sqrt{\left\lvert\sigma T_S^4\sigma(C)\right\rvert^2 + \left\lvert 4\sigma C T_S^3\sigma(T_S)\right\rvert^2}$
Transmissivity	$\sigma(\tau_T) = \lvert(3.76\cdot10^{-3}w - 22.24\cdot10^{-3})\sigma(w)\rvert$

(Bastiaanssen, 2000). In this paper we determine the Λ_i according to Gómez et al. (2005):

$$\Lambda_i = \frac{T_\mathrm{H} - T_\mathrm{S}}{T_\mathrm{H} - T_\mathrm{LE}} \tag{3}$$

where T_S is the land surface temperature, and T_H and T_LE are the temperatures corresponding to dry and wet conditions for a given albedo value (see Fig. 2). According to Roerink et al. (2000), Eq. (3) is only applicable when the atmospheric conditions are constants over the image and the study site includes simultaneously wet and dry areas. In Fig. 2 it is observed an approximately constant surface temperature (T_S) for low albedo values, related to water saturated surfaces like open water and irrigated lands, where all available energies are used in evaporation process. On the other hand, for higher albedo values the figure shows an increase of surface temperature with albedo. Thus, from A to B the temperature increase because of the change in the surface temperature is a result of less soil moisture availability yields an evapotranspiration decrease and therefore a surface temperature increase. Here surface is said to be "Evaporation controlled". Finally, surface temperature from B decreases with increasing albedo. In this point, the soil moisture decrease such as no evaporation can occur due to that all available energy is used for surface heating. Thus an albedo increase yields a net radiation decrease and therefore less surface heating. Here, surface temperature is said to be "Radiation Controlled" (see Gómez et al., 2005; Sobrino et al., 2005).

2.2. Daily evapotranspiration

Daily evapotranspiration (ET_d) is defined as the temporal integration of the instantaneous values (ET_i) according to:

$$\mathrm{ET}_d = \int_0^{24} \mathrm{ET}_i(t)\,\mathrm{d}t \tag{4}$$

The integration given by Eq. (4) cannot be applied to NOAA–AVHRR data, because several images acquired at different times in the course of the same day are needed. As LET_i is only derived once a day from remote sensing images, this integration will be done by assuming that the evaporative fraction at the daily scale is similar to that derived instantaneously from Eq. (3) at time of remote sensing data acquisition (Bastiaanssen, 2000; Farah et al., 2004). Thus writing Eq. (1) for daily and instantaneous values yields the following equation:

$$\frac{\mathrm{LET}_d}{\mathrm{LET}_i} = \frac{\Lambda_d}{\Lambda_i}\frac{(R_{nd} - G_d)}{(R_{ni} - G_i)} \approx \frac{(R_{nd} - G_d)}{(R_{ni} - G_i)} \tag{5}$$

Then ET_d may be obtained as:

$$\mathrm{ET}_d = \mathrm{LET}_i\frac{(R_{nd} - G_d)}{L(R_{ni} - G_i)} \tag{6}$$

where R_{nd} (W m^{-2}) and R_{ni} are the daily and instantaneous net radiation fluxes respectively (L is the latent heat vaporization: $L = 2.45$ MJ kg^{-1}). The change from instantaneous to daily

Table 4
Values and errors for the different quantities considered in the sensitivity analysis

Parameter	Symbol	Value	Error
Atmospheric water vapour content	W	2.9 g cm^{-2}	0.5 g cm^{-2}
Atmospheric transmittance	τ	0.670	0.006
Surface albedo	α	0.150	0.017
Ratio between the incoming and emitted longwave radiation	C	0.77	0.06
Surface emissivity	ε	0.98	0.01
Surface temperature	T_S	300.0 K	1.3 K
Modified soil adjusted vegetation index	MSAVI	0.5	0.1
Evaporative fraction	Λ	0.60	0.12
Ratio between daily and instantaneous net radiation	C_{di}	0.30	0.03

Values for the atmospheric parameters were extracted from a standard mid-latitude summer atmospheric profile. Error values were obtained from the different references given in the text.

values of net radiation may be performed using the ratio between both values ($C_{di} = R_{nd}/R_{ni}$). In this way Eq. (6) can be rewritten as:

$$\mathrm{ET}_d = \frac{\Lambda_i C_{di} R_{ni}}{L} \tag{7}$$

The hypothesis of a daily ground heat flux close to zero was also considered for deriving Eq. (7). Seguin and Itier (1983)
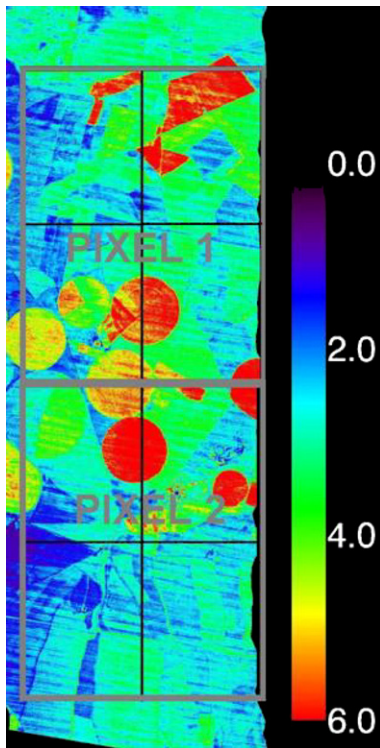

Fig. 4. Daily evapotranspiration (mm d^{-1}) obtained from the high resolution data acquired by the DAIS sensor over the agricultural area of Barrax (Albacete, Spain) on 4 June 1999. These values were used to check the method proposed in the paper for low resolution data. The NOAA–AVHRR pixels overlapped on the DAIS image are also shown.

Table 5
Daily evapotranspiration values extracted from DAIS (ET$_{DAIS}$) and NOAA AVHRR (ET$_{AVHRR}$) images acquired on 4 June 1999 for the two different regions of interest (ROI) over the Barrax area

Region of interest (ROI)	ET$_{DAIS}$ (mm d^{-1})	ET$_{AVHRR}$ (mm d^{-1})	ET$_{AVHRR}$−ET$_{DAIS}$ (mm d^{-1})
1	2.9±0.4	2.4±0.3	−0.5
2	2.7±0.3	2.4±0.4	−0.3

Mean and standard deviation values are given. According to Fig. 3, ROI 1 includes pixels from 1 to 4, and ROI 2 includes pixels from 5 to 8.

proposed a constant value $C_{di} = (0.30 \pm 0.03)$, but Wassenaar et al. (2002) showed that this ratio varied from winter (0.05) to summer (0.3) following the pattern of a sine law. In this study, C_{di} was calculated using net radiation fluxes measured in the meteorological station of the El Saler area, located in the East coast of the Iberian Peninsula (Valencia, 39° 20′ 41.165″ N, 0° 19′ 12.031″ W, at sea level). Fig. 3 shows the relationships between the ratio (C_{di}) and the day of year (DOY) at the different times used in this work (see Table 2).

3. Data

3.1. NOAA–AVHRR imagery

In this paper a total amount of 160 NOAA–AVHRR images over the Iberian Peninsula (900 × 540 pixels) was used, with an acquisition period ranging from June-1997 to November-2002 (around 30 images per year and 2 or 3 images per month) and an acquisition time near midday, from 12:00 to 15:00 GMT. The images were provided geometrically and radiometrically corrected by the Centro de Recepción, Proceso, Archivo y Distribución de Imágenes de Observación de la Tierra (CREPAD, http://www.crepad.rcanaria.es), jointly with the images of the solar zenith angle at the time of acquisition. Cloud and sea masks were also applied to the NOAA–AVHRR images, following the procedure described in Saunders and Kriebel (1988).

Table 6
Daily evapotranspiration values extracted from PolDER and Inframetrics (ET$_{POLDER-INFRAMETRICS}$) and NOAA–AVHRR (ET$_{AVHRR}$) images acquired on Alpilles test area ((*): not available data for this region and this day)

| Data (aa/mm/dd)	ET$_{POLDER-INFRAMTRICS}$ (mm d^{-1})	ET$_{AVHRR}$ (mm d^{-1})
970410	2.69	2.94
970416	1.85	1.32
970418	2.71	2.45
970501	2.86	2.45
970502	4.08	(*)
970522	2.58	3.14
970612	3.47	2.03
970624	2.28	3.01
970708	3.23	2.22
970728	3.68	2.87
970829	3.41	3.19
970904	3.16	3.99
970918	3.83	1.53
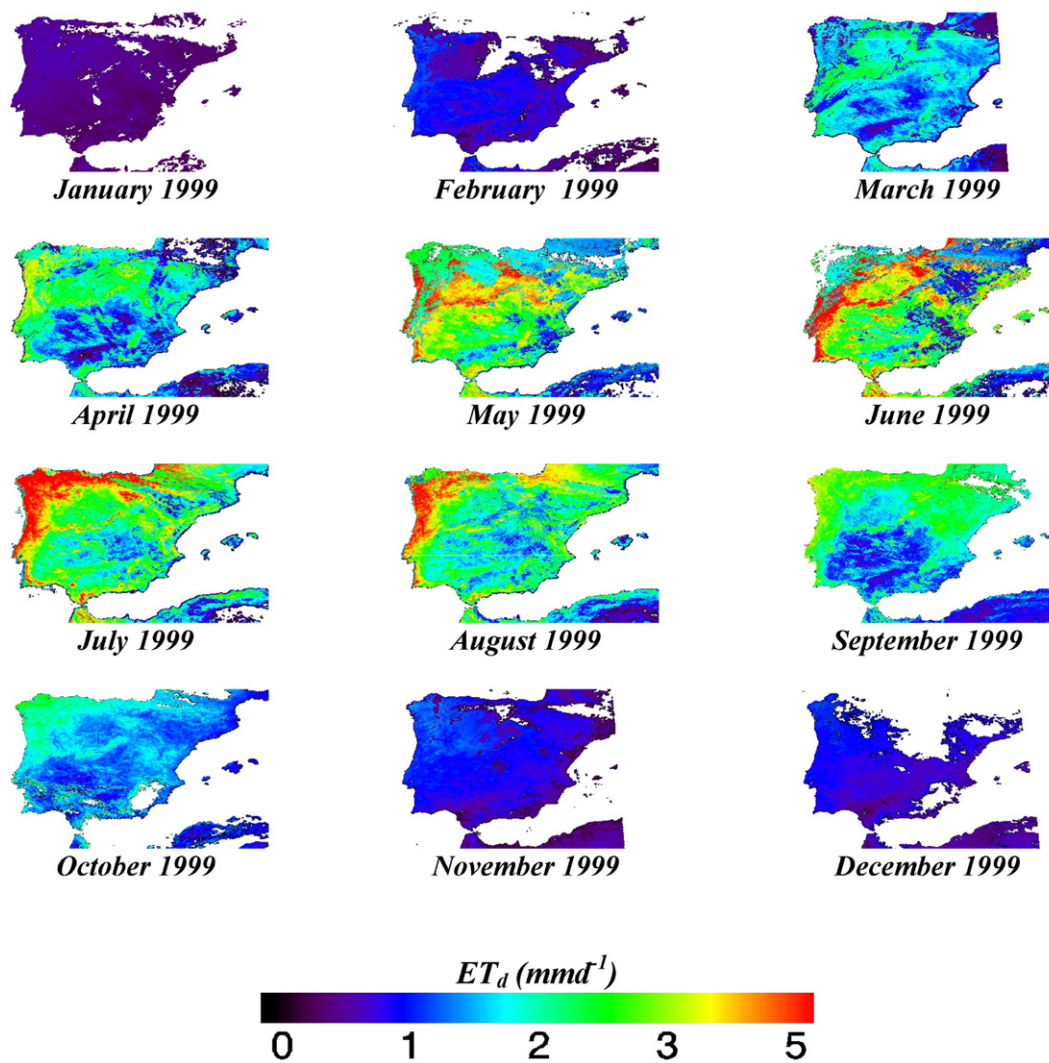
Fig. 5. Monthly mean for the daily evapotranspiration retrieved from NOAA–AVHRR data over the Iberian Peninsula in 1999. Pixels in black color refer to sea and cloud masks.

3.2. High resolution data

ET values measured in situ using meteorological stations are not representative at the NOAA–AVHRR spatial resolution (∼ 1 km). High resolution ET images were used in order to check the results obtained from AVHRR data. For this purpose, the Digital Airborne Imaging Spectrometer (DAIS) was used, with a spatial resolution of 5 m. ET retrieval from DAIS data was described in detail in Sobrino et al. (2005) and Gómez et al. (2005). To be more specific, the DAIS image acquired on June 4th 1999 over the Barrax agricultural area (Albacete, 39° 6′N, 2° 6′W; 700 m) in the framework of the DAIS Experiment (DAISEX-99) was used, which provided an error for the daily ET of 1 mm d^{-1}. It was the only available high resolution image in coincidence with the NOAA–AVHRR acquisition (see Fig. 3). In Table 1 the different equations used to estimate the daily ET to high and low resolution images was presented.

4. Results

4.1. Sensitivity analysis

A sensitivity analysis was carried out in order to assess the accuracy of the retrieved ET using the method proposed in this paper. For this purpose, the error theory had been applied similarly as in the sensitivity analysis realized in Gómez et al. (2005), using the equations showed in Table 3 with the values and errors of the variables and parameters involved in the retrieval of ET given in Table 4. The estimation of instantaneous evaporative fraction error is the critical point of the sensitivity analysis. This is due to the fact that T_H and T_{LE} are obtained from a graphical procedure which may generate significant errors. To evaluate these errors, the plot of Ts versus albedo was analysed in Gómez et al. (2005). According to the results obtained, the sensitivity analysis provided an error lower than 29 W m^{-2} for the net radiation, lower than 15 W m^{-2} for the
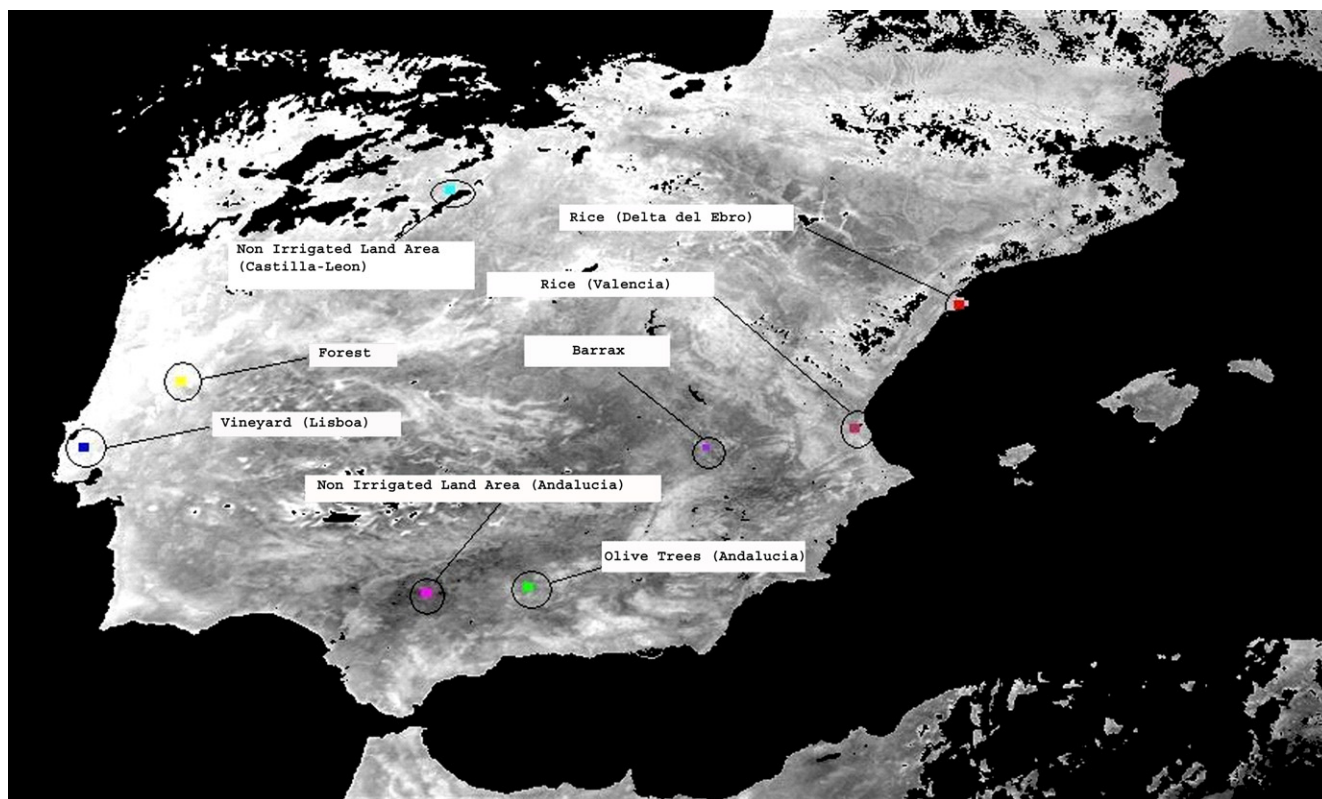
Fig. 6. Selected zones over the Iberian Peninsula to analyze the monthly and seasonal evolution of the daily evapotranspiration from 1997 to 2002.

soil heat flux, and lower than 45 W m^{-2} for the latent heat flux. The estimated error for ET was lower than 1.4 mm d^{-1}.

4.2. Test of the algorithm by comparing NOAA estimated ET and DAIS estimates

As stated in Section 3.2, the available in situ values of ET are not representative at the low spatial resolution of the AVHRR sensor, and ET values extracted from DAIS high resolution data were used in order to check the method proposed in this paper. The DAIS image includes only 2×4 NOAA–AVHRR pixels, as shown in Fig. 4. It would be possible to compare the ET values obtained in DAIS and AVHRR images in each AVHRR pixels (8 pixels) but in order to avoid the problems related with the positioning of the AVHRR pixels over the DAIS image, two regions of interest (ROI) composed by 2×2 AVHRR pixels were considered: ROI 1 included pixels 1 to 4 and ROI 2 included pixels 5 to 8, according to the notation used in Fig. 4. Mean values of ET for the ROIs were compared to the mean values obtained from the equivalent DAIS pixels (Table 5). Mean values extracted from AVHRR images were equal for the two ROIs, with low standard deviations (less than 0.4 mm d^{-1}). DAIS values were also similar for the two ROIs, but standard deviations were higher (1 mm d^{-1}; Sobrino et al., 2005) due to the heterogeneity observed from high resolution data (1 NOAA–AVHRR pixel included 280×370 DAIS pixels). Differences between AVHRR and DAIS estimates of ET were −0.5 and −0.3 mm d^{-1} for ROIs 1 and 2, respectively. Taking into account that Sobrino et al. (2005) evaluated that ET

retrieved from DAIS had an error of 1 mm d^{-1} and that the differences between NOAA and DAIS estimates were in the same range, it was possible to evaluate an overall error as given by $\sqrt{1^2 + 1^2} = 1.4$ mm d^{-1}, which agreed with the result obtained in the sensitivity analysis described in Section 4.1.

ET estimated from NOAA–AVHRR data was also compared with PolDER (Polarization and Directionality of Earth Reflectance) and Inframetrics Thermal Camera ET images over the Alpilles area (see Gómez et al., 2005). To realize this analysis, the area included in the PolDER and Inframetrics images has been selected in the NOAA Alpilles images, and then the daily evapotranspiration values have been extracted (see Table 6) and compared. As a result of this comparison, an RMSE around 1.4 mm d^{-1} has been obtained for the daily evapotranspiration obtained with NOAA–AVHRR images, which agreed with the results obtained previously in the sensitivity analysis.

4.3. Temporal evolution

NOAA–AVHRR images acquired from June 1997 to November 2002 were used in order to analyze monthly and seasonal evolutions of the daily evapotranspiration. Monthly values of ET were obtained by averaging the daily ET images for a given month and were given in mm d^{-1}. Seasonal ET was obtained by averaging daily ET over the season. As an example, Fig. 5 shows monthly ET maps obtained from the NOAA–AVHRR images acquired in 1999.

Fig. 5 shows that the highest ET values were obtained in summer and spring in the North and West of the Iberian
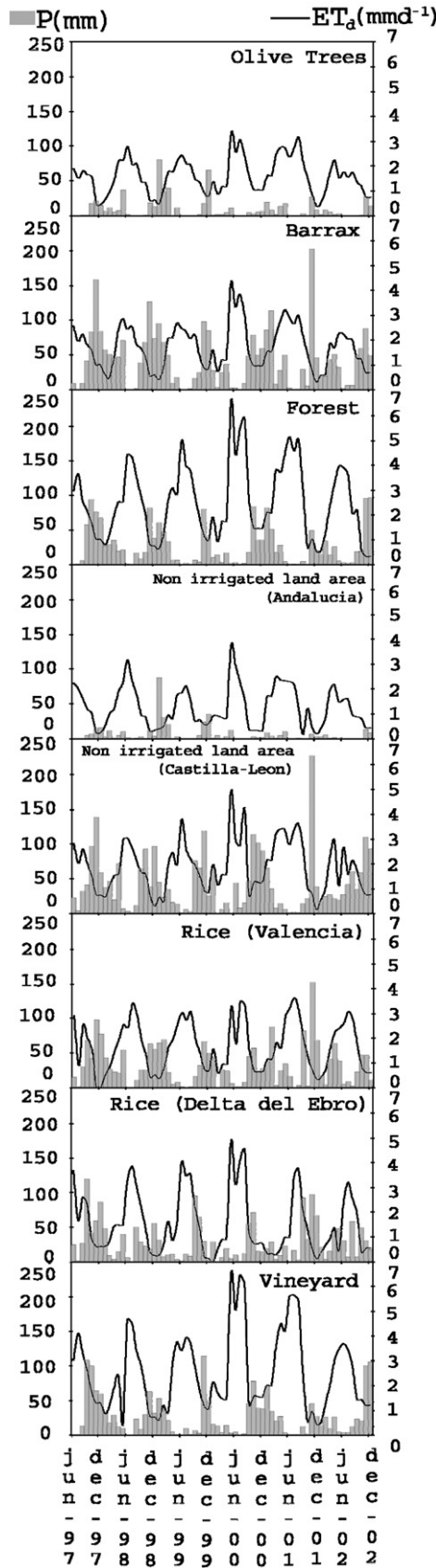
Fig. 7. Monthly evolution (from June 1997 to November 2002) of the daily evapotranspiration (ET_d) and precipitations (mm) in the eight selected zones (see Fig. 4).

Peninsula, since these areas are highly vegetated and have lowest surface temperatures. During the other seasons (October to February), ET was lower and the spatial variation decreased. This was in agreement with the seasonal variations of the amount of incoming solar radiation and with the distribution of rains among the peninsula.

The temporal analysis has been focused in eight areas of the Iberian Peninsula with different land use: rice (Delta del Ebro and Valencia), olive trees (Andalucía), vineyard (Lisboa), forest (Portugal), non irrigated land (Castilla-León and Andalucía) and the agricultural area of Barrax (see Fig. 6).

Fig. 7 shows the evolution of the monthly ET and monthly precipitation obtained by Reanalysis for the different areas between June 1997 and November 2002. In general, the highest evapotranspiration rates were obtained in 2000 and 2001, with a higher ET in summer in 2000. As expected, the highest values of ET were obtained in Spring and Summer. In the western areas (vineyard and forest) the highest values of ET were obtained in spring and summer, which can be explained according to the rain gradient from the Atlantic Ocean. In general, the high rain in winter and spring is responsible for high ET, and in summer, vegetation has a lot of available water in the soil because of the previous high rain. In April, June and July 2000 values close to 6 mm d^{-1} were found in these areas.

The lowest ET values were obtained in winter for all areas (in general close to 1 mm d^{-1}). In Spring and Summer, the non irrigated lands or partially irrigated area presented the lowest ET. In Spring, the rice areas (Valencia, Ebro) exhibited ET rates close to ET in the non irrigated or partially irrigated area, while their ET increased significantly in summer, certainly in relation with the large availability of water for rice in summer due to flooding.

Also Fig. 7 shows the relation between ET and available soil water due to the precipitation. In months with high precipitation values, we observed low ET values due to the low incoming radiation values, but two or three months later the daily ET values increase due to the high available water in the soil as a consequence of the previous precipitations.

The seasonal evolution is more clearly shown in Fig. 8, in which the seasonal daily ET is graphed for the different areas and years (from 1997 to 2002). Fig. 8 shows that vineyard have the highest ET values in summer–autumn as a consequence of large amount of leaves in the crop. In against, the lower values of ET are associated with the winter, when the crop does not have leaves. In Barrax area the higher values are presented in spring and summer where crops such as corn are in the highest development, and the lower values are associated with the winter.

5. Conclusions

In this paper, the method suggested by Sobrino et al. (2005) and Gómez et al. (2005) for ET retrieval from high spectral and spatial resolution data (∼5 m) was adapted to the low resolution data provided by the NOAA–AVHRR sensor (∼1 km). The method is based on the evaporative fraction concept developed by Roerink et al. (2000). The principal advantage of the proposed methodology is that the method requires only satellite
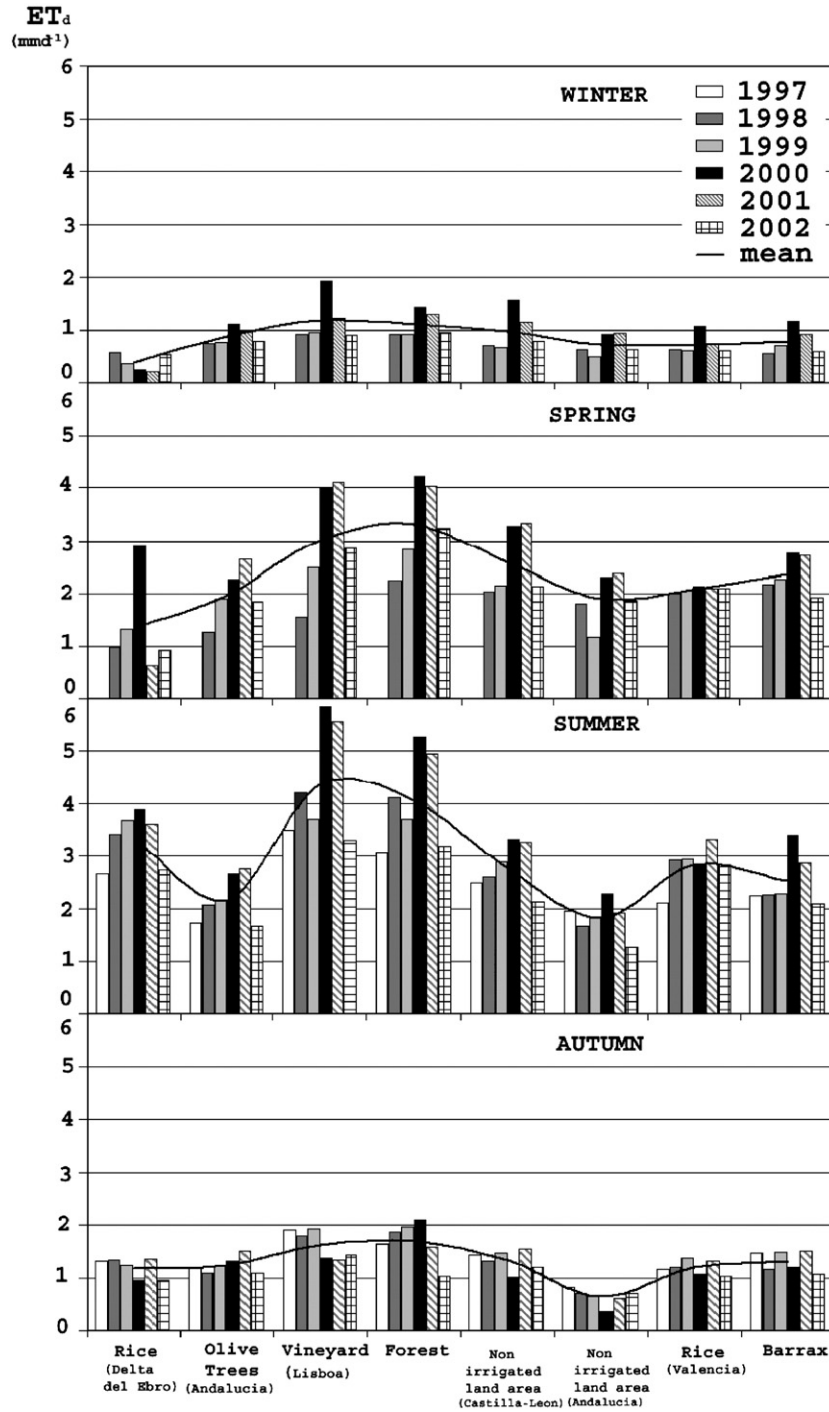
Fig. 8. Monthly evolution (from June 1997 to November 2002) of the daily evapotranspiration (ET$_d$) in the eight selected zones (see Fig. 4). The temporal mean for the six selected years is also graphed.

data, so it is easy to implement and allows to estimate the ET in areas without measurements. However, the principal disadvantage of the methodology is that the studied images must contain extreme surface values temperature.

The study was focused on the Iberian Peninsula, and a temporal set of NOAA–AVHRR images acquired from 1997 to 2002 has been used. The method was checked over an agricultural area (Barrax, Albacete, Spain) using the high resolution values presented in Sobrino et al. (2005), with errors lower than 1.4 mm d^{-1}, which agreed also with the sensitivity analysis.

The monthly and seasonal evolution of ET was also analyzed. The highest values of ET (~ 6 mm d^{-1}) were obtained in the West of the Iberian Peninsula, which is the most vegetated area. The impact of incoming solar energy was also noticed, with higher values of ET in Spring and Summer and lower values in Autumn and Winter.

Acknowledgements

References

Abreu, L. W., & Anderson, G. P. (Eds.). (1996). *The MODTRAN 2/3 Report and LOWTRAN 7 MODEL, Modtran Report, Contract F19628-91-C-0132*.

Bastiaanssen, W. G. M. (2000). SEBAL-based sensible and latent heat fluxes in the irrigated Gediz Basin, Turkey. *Journal of Hydrology, 229*, 87−100.

Bastiaanssen, W. G. M., Menenti, M., Feddes, R. A., & Holtslag, A. A. M. (1998). A remote sensing surface energy balance algorithm for land (SEBAL). 1. Formulation. *Journal of Hydrology, 212–213*, 198−212.

Bastiaanssen, W. G. M., Pelgrum, H., Wang, J., Ma, Y., Moreno, J. F., & Roerink, G. J. (1998). A remote sensing surface energy balance algorithm for land (SEBAL). Part 2: Validation. *Journal of Hydrology, 212–213*, 213−229.

Farah, H. O., Bastiaanssen, W. G. M., & Feddes, R. A. (2004). Evaluation of the temporal variability of the evaporative fraction in a tropical watershed. *International Journal of Applied Earth Observation and Geoinformation, 5*, 129−140.

French, A., Schmugge, T. J., Kustas, W. P., Brubaker, K. L., & Prueger, J. (2003). Surface energy fluxes over El Reno, Oklahoma using high resolution remotely sensed data. *Water Resources Research, 39*, 1164.

Gillespie, A. R. (1985). Lithologic mapping of silicate rocks using TIMS. *The TIMS Data User's Workshop, JPL Pub., 86-38* (pp. 29−44).

Gómez, M., Sobrino, J. A., Olioso, A., & Jacob, F. (2005). Retrieval of evapotranspiration over the Alpilles/ReSeDA experimental site using airborne POLDER sensor and Thermal Camera. *Remote Sensing of Environment, 96*(3–4), 399−408.

Hurtado, E., & Sobrino, J. A. (2001). Daily net radiation estimated from air temperature and NOAA−AVHRR data: A case study for the Iberian Peninsula. *International Journal of Remote Sensing, 22*(8), 1521−1533.

Jacob, F., Olioso, A., Gu, X. F., Su, Z., & Seguin, B. (2002). Mapping surface fluxes using airborne visible, near infrared, thermal infrared remote sensing data and a spatialized surface energy balance model. *Agronomie, 22*, 669−680.

Jia, L., Su, Z., Van der Hurk, B., Menenti, M., Moene, A., De Bruin, H. A. R., et al. (2003). Estimation of sensible heat flux using the Surface Energy Balance System (SEBS) and ATSR measurements. *Physics and Chemistry of the Earth, 28*(1–3), 75−88.

Kustas, W. P., & Norman, J. M. (1999). Evaluation of soil and vegetation heat flux predictions using a simple two-source model with radiometric temperatures for partial canopy cover. *Agricultural and Forest Meteorology, 94*, 13−29.

Li, Z. -L., Jia, L., Su, Z., Wan, Z., & Zhang, R. (2003). A new approach for retrieving precipitable water from ATSR2 split-window channel data over land area. *International Journal of Remote Sensing, 24*(24), 5095−5117.

Norman, J. M., Kustas, W. P., & Humes, K. S. (1995). Two source approach for estimating soil and vegetation energy fluxes in observations of directional radiometric surface temperature. *Agricultural and Forest Meteorology, 77*, 263−293.

Roerink, G. J., Su, Z., & Menenti, M. (2000). S-SEBI: A simple remote sensing algorithm to estimate the surface energy balance. *Physics and Chemistry of the Earth. Part B: Hydrology, Oceans and Atmosphere, 25*(2), 147−157.

Saunders, R. W., & Kriebel, K. T. (1988). An improved method for detecting clear sky and cloudy radiances from AVHRR data. *International Journal of Remote Sensing, 9*, 123−150.

Seguin, B., & Itier, B. (1983). Using midday surface temperature to estimate daily evaporation from satellite thermal IR data. *International Journal of Remote Sensing, 4*(2), 371−383.

Sobrino, J. A., Gómez, M., Jiménez-Muñoz, J. C., Olioso, A., & Chehbouni, G. (2005). A simple algorithm to estimate evapotranspiration from DAIS data: Application to the DAISEX Campaigns. *Journal of Hydrology, 315*, 117−125.

Sobrino, J. A., Jiménez-Muñoz, J. C., Labed-Nachbrand, J., & Nerry, F. (2002). Surface emissivity retrieval from Digital Airborne Imaging Spectrometer data. *Journal of Geophysical Research, 107*(D23), 4729. doi:10.1029/2002JD002197

Sobrino, J. A., Li, Z. -L., & Stoll, P. (1993). Impact of the atmospheric transmittance and total water vapor content in the algorithms for estimating satellite sea surface temperatures. *IEEE Transactions on Geoscience and Remote Sensing, 31*, 946−952.

Sobrino, J. A., Li, Z. L., Stoll, M. P., & Becker, F. (1994). Improvements in the split-window technique for land surface temperature determination. *IEEE Transactions on Geoscience and Remote Sensing, 32*, 243−253.

Sobrino, J. A., & Raissouni, N. (2000). Toward remote sensing methods for land cover dynamic monitoring. Application to Morocco. *International Journal of Remote Sensing, 20*(2), 353−366.

Sobrino, J. A., Raissouni, N., Simarro, J., Nerry, F., & François, P. (1999). Atmospheric water vapor content over land surfaces derived from the AVHRR Data. Application to the Iberian Peninsula. *IEEE Transactions on Geoscience and Remote Sensing, 37*, 1425−1434.

Su, Z. (2002). The surface energy balance system (SEBS) for estimation of turbulent heat fluyes. *Hydrology and Earth System Sciences, 6*(1), 85−99.

Wassenaar, T., Olioso, A., Hasager, C., Jacob, F., & Chehbouni, A. (2002). Estimation of evapotranspiration on heterogeneous pixels. In J. A. Sobrino (Ed.), *First International Symposium on Recent Advances in Quantitative Remote Sensing, 16–20 September 2002, Valencia, Spain* (pp. 458−465). España: Publications de la Universitat de València.